Growth of Au−Pd2Sn Nanorods via Galvanic Replacement and Their Catalytic Performance on Hydrogenation and Sonogashira Coupling Reactions

Raquel Nafria,†,∇ Zhishan Luo,†,∇ Maria Ibañez,‡,§ Sara Martí-Sanchez, ∥ Xiaoting Yu,† Maria de la Mata,∥ Jordi Llorca,⊥ Jordi Arbiol,∥,# Maksym V. Kovalenko,‡,§ Arnald Grabulosa,*,¶ Guillermo Muller,¶ and Andreu Cabot*,†,#

† Catalonia Institute for Energy Research (IREC), 08930 Sant Adriàde Besos, Barcelona, Spain

‡ Institute of Inorganic Chemistry, Department of Chemistry and Applied Biosciences, ETH Zürich, Zürich CH-8093, Switzerland § Empa-Swiss Federal Laboratories for Materials Science and Technology, Dübendorf CH-8600, Switzerland

∥ Catalan Institute of Nanoscience and Nanotechnology (ICN2), CSIC and the Barcelona Institute of Science and Technology (BIST), Campus UAB, Bellaterra, 08193 Barcelona, Spain

⊥Institut de Tecniques Energètiques, Universitat Politècnica de Catalunya, 08028 Barcelona, Spain

ICREA, Pg. Lluís Companys 23, 08010 Barcelona, Spain

¶ Departament de Química Inorganica i Orgànica, Seccioó de Química Inorgànica, Universitat de Barcelona, Martí i Franquès 1-11, 08028 Barcelona, Spain

ABSTRACT

Colloidal Pd2Sn and Au−Pd2Sn nanorods (NRs) with tuned size were produced by the reduction of Pd and Sn salts in the presence of size- and shape-controlling agents and the posterior growth of Au tips through a galvanic replacement reaction. Pd2Sn and Au−Pd2Sn NRs exhibited high catalytic activity toward quasi-homogeneous hydrogenation of alkenes (styrene and 1-octene) and alkynes (phenylacetylene and 1-octyne) in dichloromethane. Au− Pd2Sn NRs showed higher activity than Pd2Sn for 1-octene, 1- octyne, and phenylacetylene. In Au−Pd2Sn heterostructures, X-ray photoelectron spectroscopy evidenced an electron donation from the Pd2Sn NR to the Au tips. Such heterostructures showed distinct catalytic behavior in the hydrogenation of compounds containing a triple bond such as tolan. This can be explained by the aurophilicity of triple bonds. To further study this effect, Pd2Sn and Au−Pd2Sn NRs were also tested in the Sonogashira coupling reaction between iodobenzene and phenylacetylene in N,N-dimethylformamide. At low concentration, this reaction provided the expected product, tolan. However, at high concentration, more reduced products such as stilbene and 1,2-diphenylethane were also obtained, even without the addition of H2. A mechanism for this unexpected reduction is proposed.

1. INTRODUCTION

Multimetallic catalysts have associated several potential advantages over elemental compositions, including1−4 (i) cost reduction associated with the utilization of lower amounts of noble metals; (ii) additional degrees of freedom to tune the electronic structure toward the creation of suitable adsorption/ reaction sites; (iii) close location of different adsorption/ reaction sites enabling tandem reactions that potentially reduce the number of synthetic steps toward a specific product; and (iv) allow for alternative multisite reaction paths that may be faster, more selective, and/or prevent poisoning species to be formed or to remain at the catalyst surface.

Multimetallic catalysts can be realized by several methods including the incorporation of multiple metallic centers within a molecule or the impregnation of the different metals on a high surface area support. However, a particularly interesting and at the same time underexploited class of catalysts is that of size-, shape-, and compositional-engineered multimetallic colloidal nanoparticles (NPs). Being unsupported, essentially solution-dispersed, colloidal NPs combine the advantages of classic homogeneous and heterogeneous catalysts;5−12 like catalytic organic molecules, colloidal NPs can be produced with extraordinary control over chemical and structural parameters, potentially enabling the rational engineering of their catalytic activity and especially selectivity in sensitive reactions.12−16 Colloidal NPs also have extremely high surfaceto-volume ratios, which makes them potentially very active. Additionally, unlike molecular catalysts, NPs are easily separated from the solvent, reactants, and products, preventing product contamination and allowing catalyst reutilization in multiple cycles. Multimetallic colloidal NPs are typically prepared by the coreduction or thermal decomposition of precursors of the different metals and/or the heteronucleation of a second or third compound at the surface of a preformed NP. Additionally, atomic substitution reactions can be used to partially or totally modify the stoichiometry of preformed NPs obtaining new and eventually much more complex compositions. In this direction, galvanic replacement reactions, involving the substitution of lattice atoms by ions in solution mediating a redox reaction, are particularly suitable.17−22 The galvanic replacement is driven by a difference in reduction potential between the replacing and replaced elements, which allows the reaction to proceed at moderate temperatures and minimizing homonucleation of independent NPs. However, in spite of its high potential and versatility, very few examples exist on the modification of the composition of multimetallic nanostructures by a galvanic replacement reaction.23,24

The development of catalysts for organic reactions is driven by the search for cost-effective and environmentally friendly processes suitable for a sustainable society. From the myriad of currently exploited catalytic reactions, hydrogenation and cross-coupling are among the most heavily studied. Hydrogenation comprises an exceedingly important group of reactions, including the Haber−Bosch process as well as the reduction of alkenes, aldehydes, ketones, and imines.25 On the other hand, cross-coupling reactions comprise several essential mechanistically related reactions, including Suzuki, Stille, Heck, and Sonogashira couplings among others.26 Although numerous homo- and heterogeneous catalysts have been successfully applied in these reactions, several performance, economic, and impact parameters, such as activity, selectivity, substrate scope, durability/recyclability, cost effectiveness, environmental friendliness, and sustainability require further improvement, making the design of better hydrogenation and cross-coupling catalysts a worth endeavor.

Pd-based multimetallic catalysts and particularly Pd−Sn alloys have raised especial attention in these reactions owing to their reduced cost and improved performance compared to bare Pt or

Pd catalysts.16,26−31 We recently described the synthesis of Pd2Sn nanorods (NRs) with narrow size distribution and geometry control.16 In the present paper, we report a procedure based on a galvanic replacement reaction for the growth of Au tips onto Pd2Sn NRs to produce Au− Pd2Sn heterostructured NRs. With both types of NRs in hand, we compare the performance of Pd2Sn and Au−Pd2Sn NPs in alkene and alkyne hydrogenations and in Sonogashira couplings. These reactions have been chosen because Pd−Sn systems have previously shown excellent performances28 and there is also literature precedents demonstrating that supported Au NPs are active both in hydrogenation32 and Sonogashira33−38 couplings because of the aurophilicity of alkynes.39−41

2. EXPERIMENTAL SECTION

2.1. Chemicals.

Palladium(II) acetylacetonate ([Pd(acac)2], 99%), tin(II) acetate (Sn(OAc)2), gold(III) chloride (AuCl3, 99.99%), 1-octadecene (ODE, 90%), methylamine hydrochloride (MAHC), oleylamine (OAm, >70%), hydrochloric acid (37% in water), styrene, 1-octene, phenylacetylene (PhA), 1-octyne, tolan, iodobenzene (PhI), potassium carbonate, and potassium hydroxide were purchased from Sigma-Aldrich. Tri-n-octylphosphine (TOP, 97%) was acquired from Strem. Analytical grade hexane, chloroform, N,N-dimethylformamide (DMF), dichloromethane (DCM), toluene, and ethanol were obtained from various sources. All chemicals were used as received, except OAm, which was purified by distillation.

2.2. Synthesis of Pd2Sn NRs.

Pd2Sn NRs were produced following our previous report16 with a slight modification to improve the product yield while simultaneously using an air-stable reactant, Sn(OAc)2, instead of the air-sensitive tin(II) acetylacetonate used previously. In a typical synthesis, 20 mL of OAm, 0.8 mmol MAH, 0.3 mmol [Pd(acac)2], and 0.15 mmol Sn(OAc)2 were placed in a 100 mL four-neck flask and purged under argon flow for 30 min at 60 °C. Then, 1 mL of TOP was injected into the solution and the mixture was heated to 200 °C at 12 °C/min. After maintaining the reaction mixture at 200 °C for 30 min, the solution was heated to 300 °C at 2.5 °C/min and maintained for additional 30 min at this temperature. Finally, the solution was cooled down and Pd2Sn NRs were separated from the reaction mixture by adding 20 mL of ethanol and centrifuging at 3000 rpm for 5 min. NRs were washed with chloroform as the solvent and ethanol as the nonsolvent by two precipitation/redispersion steps. With the adjustment of MAHC amount, different sizes and aspect ratios of Pd2Sn NRs were obtained, following our previous report:16 26 ± 2 nm × 9 ± 1 nm (0.85 mmol MAHC) and 40 ± 5 nm × 11 ± 2 nm (0.9 mmol MAHC).

2.3. Synthesis of Au−Pd2Sn NRs.

Au−Pd2Sn NRs were prepared by growing Au over Pd2Sn NRs produced following the procedure described above. Initially, a fresh stock solution was prepared in a glovebox containing 0.02 mmol AuCl3 in 50 μL of OAm and 2 mL of ODE. Then, this Au stock solution was injected at room temperature into 5 mL of Pd2Sn NRs dispersed in toluene (5 mg/ mL) under strong stirring and maintained in these conditions for 60 min. Finally, Au−Pd2Sn NRs were washed by multiple precipitation/ redispersion using toluene and ethanol. When different amounts of Au stock solution were used, different Au contents were obtained in the Pd2Sn NRs. For too high amounts, >0.04 mmol, significant amounts of Au homogeneously nucleated in the solution.

2.4. Procedures for the Catalytic Runs.

2.4.1. Hydrogenation Reactions. An exactly weighted quantity of 10 nm Pd2Sn or 12 nm Au−Pd2Sn NRs (usually 10.0 mg) and the allotted quantity of the substrate (styrene, 1-octene, PhA, 1-octyne, or tolan) were dissolved in 20 mL of the solvent of choice under a nitrogen atmosphere, sonicated for 10 minutes, and transferred by a syringe to a FischerPorter flask, which was then purged with H2 three times, pressurized to the desired H2 pressure (usually 3 bar), and left stirring for the selected time.

2.4.2. Sonogashira Coupling Reactions. An exactly weighted quantity of 10 nm Pd2Sn or 12 nm Au−Pd2Sn NRs (usually 10.0 mg), PhI (204 mg, 1.0 mmol), PhA (153 mg, 1.5 mmol), and base (2 mmol) were dissolved in 10 mL of dry DMF under a nitrogen atmosphere, sonicated for 10 min, and transferred by a syringe to a microwave tube. The reaction mixture was heated to 130 °C for the allotted time. The conversions in Sonogashira coupling reactions were calculated with respect to the limiting agent (PhI). The turnover frequencies (TOFs) were calculated from the amount of product produced in a specific time interval in hours by considering the total Pd amount according to: TOF = (mol product)/(mol Pd·t)

Gas chromatography (GC) analyses after catalytic runs were performed with Agilent Technologies 6890N chromatograph equipped with a HP5-5MS capillary column (30 m × 0.32 mm size) and a flame ionization detector (FID) detector, with He as a carrier gas. Additionally, some compounds were characterized by GC−MS analyses in Agilent Technologies chromatograph 7820A with a mass detector 5975 using the same column.

2.5. Characterization.

The size and shape of initial NPs were examined by transmission electron microscopy (TEM) using ZEISS LIBRA 120, operating at 120 kV. Structural and compositional characterization of the nanocomposites were analyzed by highresolution TEM (HRTEM) and high-angle annular dark field (HAADF) scanning TEM (STEM) using a field emission gun FEI Tecnai F20 microscope at 200 kV with a point-to-point resolution of 0.19 nm. Scanning electron microscopy (SEM) analysis was carried out in a ZEISS Auriga microscope with an energy dispersive X-ray spectroscopy (EDXS) detector at 20 kV to study the chemical composition of NPs. For SEM characterization, NPs were dissolved in chloroform and were drop-casted on silicon substrates. X-ray power diffraction (XRD) patterns were obtained on a Bruker AXS D8 ADVANCE diffractometer, using Cu Kα radiation (λ = 1.5406 Å), operating at 40 kV and 40 mA, and with a LynxEye linear positionsensitive detector used in reflection geometry. For XRD characterization, the samples were deposited on a Si substrate. Ultraviolet− visible (UV−vis) spectra were recorded on a LAMBDA 950 UV−vis spectrophotometer from PerkinElmer. X-ray photoelectron spectroscopy (XPS) was performed on a SPECS system equipped with an Al anode XR50 source operating at 150 mW and a Phoibos 150 MCD-9 detector. The pressure in the analysis chamber was always below 10−7 Pa. The area analyzed was about 2 mm × 2 mm. The pass energy of the hemispherical analyzer was set at 25 eV, and the energy step was set at 0.1 eV. Data processing was performed with the CasaXPS program (Casa Software Ltd., UK). Binding energy (BE) values were centered using the C 1s peak at 284.8 eV. The atomic fractions (%) were calculated using peak areas normalized on the basis of acquisition parameters after background subtraction, experimental sensitivity factors, and transmission factors provided by the manufacturer. Thermogravimetric analyses (TGA) were performed in the temperature range of 30−500 °C at a heating rate of 10 °C min−1 under Ar using PerkinElmer TGA4000. Nuclear magnetic resonance (NMR) measurements were recorded on a Bruker AVANCE III HD Spectrometer operating at a 1 H frequency of 500.26 MHz and equipped with a BBFO-Z probe. The sample temperature was set to 298.2 K. One-dimensional (1D) 1 H and twodimensional (2D) nuclear Overhauser effect

spectroscopy (NOESY) spectra were acquired using standard pulse sequences from the Bruker library. For the quantitative 1D 1 H measurements, 64k data points were sampled with the spectral width set to 20 ppm and a relaxation delay of 30 s. NOESY mixing time was set to 300 ms and 4096 data points in the direct dimension for 512 data points in the indirect dimension were typically sampled, with the spectral width set to 10 ppm. Diffusion measurements [2D diffusion-ordered spectroscopy (DOSY)] were performed using a double stimulated echo sequence for convection compensation and with monopolar gradient pulses.44 Smoothed rectangle gradient pulse shapes were used throughout. The gradient strength was varied linearly from 2 to 95% of the probe maximum value in 64 increments, with the gradient pulse duration and diffusion delay optimized to ensure a final attenuation of the signal in the final increment of less than 10% relative to the first increment. For 2D processing, the spectra were zero-filled until a 4096−2048 real data matrix. Before Fourier transformation, the 2D spectra were multiplied with a squared cosine bell function in both dimensions, and the 1D spectra were multiplied with an exponential window function. The diffusion coefficients were obtained by fitting the appropriate Stejskal−Tanner (ST) equation to the signal intensity decay.43

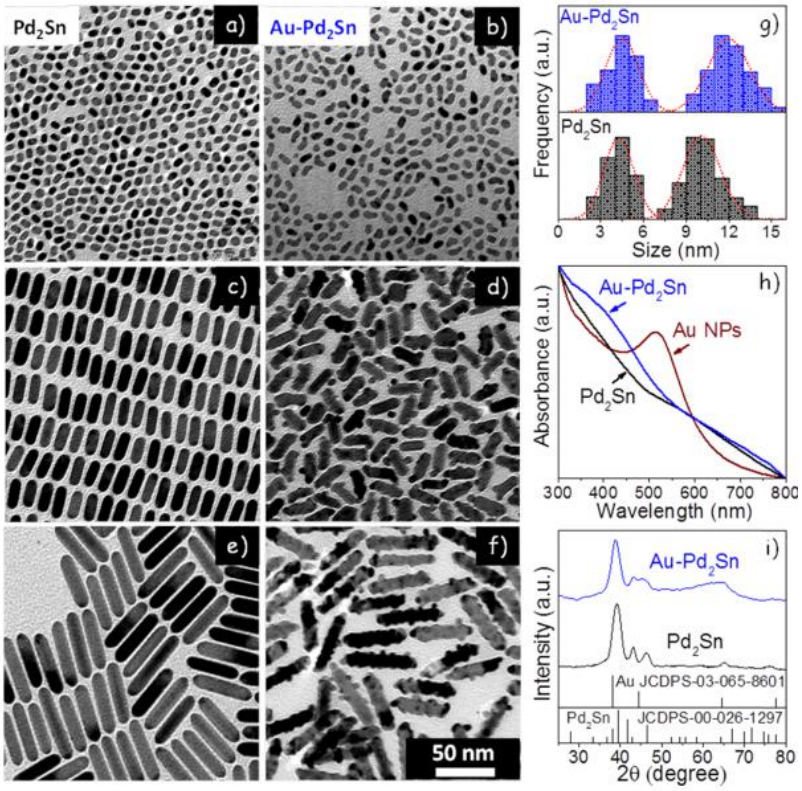

Figure 1. (a−f) TEM micrographs of Pd2Sn (a,c,e) and Au−Pd2Sn (b,d,f) NRs with three different sizes: 10 ± 2 nm × 4 ± 1 nm (a,b); 26 ± 2 nm × 9 ± 1 nm (c,d); and 40 ± 5 nm × 11 ± 2 nm (e,f). All TEM micrographs have the same scale. (g) Size distribution histograms of the smallest Pd2Sn and Au−Pd2Sn NRs. (h) UV−vis spectra of colloidal 3.5 nm Au NPs (produced by reducing AuCl3 in the absence of Pd2Sn NRs), 10 nm Pd2Sn NRs, and 12 nm Au−Pd2Sn NRs (produced from 10 nm Pd2Sn NRs). (i) XRD patterns of 10 nm Pd2Sn NRs and 12 nm Au−Pd2Sn NRs, including reference patterns for Pd2Sn and Au.

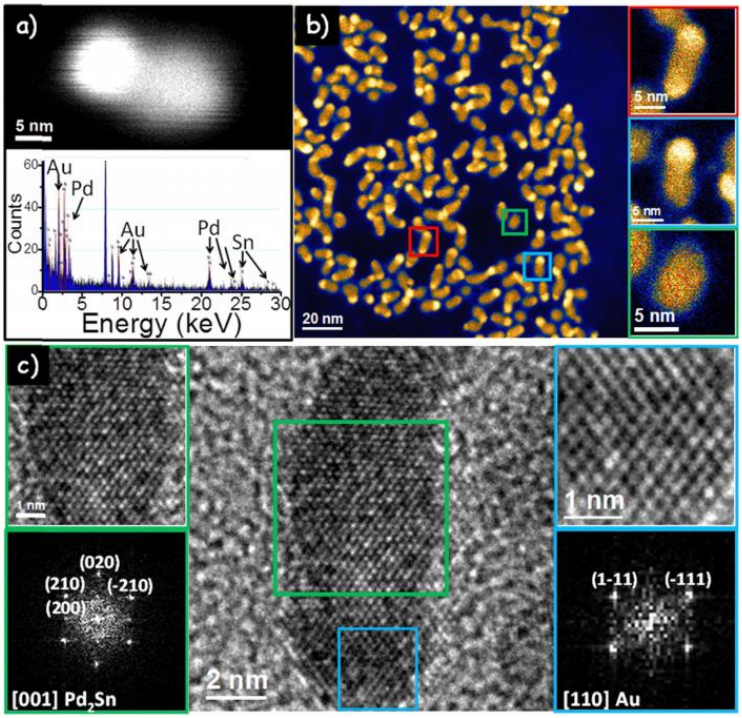

Figure 2. (a) HAADF-STEM image of a single Au−Pd2Sn NR and its corresponding EDXS spectrum. (b) Colored HAADF-STEM image of Au− Pd2Sn NRs and details of three different NRs, one containing higher contrast dots at both ends, another at only one end (most common case), and another without any higher contrast region. (c) HRTEM micrograph of a single Au−Pd2Sn NR, details of the squared regions and their corresponding power spectra.

3. RESULTS AND DISCUSSION

3.1. Structural and Chemical Properties of Pd2Sn and Au−Pd2Sn NRs.

Representative TEM micrographs of rodshaped Pd2Sn NPs with three different sizes (10 ± 2 nm × 4 ± 1 nm; 26 ± 2 nm × 9 ± 1 nm; and 40 ± 5 nm × 11 ± 2 nm) produced following the methodology detailed in the Experimental Section are shown in Figure 1a,c,e. NRs showed narrow size distributions and no apparent aggregation. Au−Pd2Sn heteronanostructures were produced by injecting, at room temperature, a solution containing 0.02 mmol AuCl3 in 50 µL of OAm and 2 mL of ODE into 5 mL of a toluene dispersion of Pd2Sn NRs (5 mg/mL) under strong stirring. After 60 min of reaction, multiple Au dots with average size of ca. 2 nm were grown along the whole NR surface for the larger NRs and preferentially at the NR ends in the smallest ones (Figure 1b,d,f). Figure 1g shows the size distribution histograms of the smallest Pd2Sn (10 ± 2 nm) and Au−Pd2Sn NRs produced. Because of the preferential growth of the Au domains at the NR tips, a slight increase of the NR length was obtained in this sample, from 10 ± 2 nm × 4 ± 1 nm to 12 ± 2 nm × 4 ± 1 nm. EDXS spectra of single Au− Pd2Sn NRs confirmed the presence of the three elements, Pd, Sn, and Au (Figure 2a). Moreover, UV−vis spectroscopy showed the disappearance of the characteristic Au plasmonic peak, suggesting a strong electronic interaction between Au and Pd2Sn nanodomains (Figure 1h). Different amounts of the Au stock solution resulted in proportional contents of Au on the surface of Pd2Sn NRs (Figure S1, Table 1). However, too high amounts, >0.04 mmol, yielded a large concentration of Au NPs homogeneously nucleated in the solution. HAADF-STEM images of the 12 nm Au−Pd2Sn NRs further confirmed the presence of

Au dots at the Pd2Sn NR tips, as deduced by the brighter dots associated to the higher Z contrast of Au (Figure 2). Even though most of the NRs showed the presence of Au in just one tip, a few contained Au on both sides of the NR, whereas a few other displayed no contrast difference. XRD patterns showed Pd2Sn NRs to have an orthorhombic crystal structure (JCPDS no. 00-026-1297).

Table 1. Atomic Ratios of 10 nm Pd_2Sn and 12 nm Au−Pd_2Sn NRs As Obtained by EDXS and XPS Analyses and Atomic Percentage of Each Oxidation State As Obtained from the Fitting of the XPS Spectra

$[AuCl_3]$ M	[Pd]/[Sn]	[Au]/[Pd]	[Pd]/[Sn]	[Au]/[Pd]	Pd^0 at. %	Pd^{2+} at. %	Sn^0 at. %	Sn^{2+} at. %	Sn^{4+} at. %	Au^0 at. %	$Au^{\delta+}$ at. %
	EDXS		XPS								
	2.0		1.25		79.4	20.6	21.7	70.2	8.0		
0.01	2.2	0.07									
0.02	2.3	0.14	5.5	0.5	86.2	13.8	18.4	81.7		61.9	38.1
0.04	2.4	0.26									

The Au XRD reflections were mostly hidden by the Pd2Sn peaks, but slight shoulders at 2θ = 44.5° and 64.5° and a shift of the main Pd2Sn diffraction peak to lower angles suggested the presence of Au crystalline domains (Figure 1i). HRTEM analysis confirmed the orthorhombic crystal structure of Pd2Sn NRs (space group Pnma) with a = 5.65 Å, b = 4.31 Å, and c = 8.12 Å, showing [010] as the NR growth direction and revealing the presence of Au crystal domains at the Pd2Sn NR tips (Figure 2c). The Au crystal phase was identified as cubic Fm3̄m with a = b = c = 4.09 Å. Within this face, the Au{111} and Pd2Sn{210} planes, as well as Au{002} and Pd2Sn{020} present almost identical lattice parameters, which allowed both structures to form an almost perfect epitaxy.

Within its experimental error, EDXS analysis of 10 nm Pd2Sn NRs showed the atomic ratio of Pd and Sn to be consistent with stoichiometric Pd2Sn ([Pd]/[Sn] = 2.0 ± 0.1). However, with the introduction of Au, higher Pd ratios were systematically obtained as detailed in Table 1. We associate this experimental observation to a galvanic replacement of Sn by Au. When adding AuCl3 to the solution containing Pd2Sn NRs, Au3+ ions in solution were reduced to Au+ or even Au0 at the NR surface through the simultaneous oxidation of Sn or Sn2+ ions to Sn4+ and the subsequent solvation of Sn4+ ions in the solution containing the remaining chlorine ions. Au+ could be also further reduced to Au0 through charge transfer from Pd atoms (Figure 3a).23

To further clarify the composition and oxidation states of the different elements within Pd2Sn and Au−Pd2Sn NRs, samples were analyzed using XPS (Figure 3b−f). In 10 nm Pd2Sn NRs, the atomic ratio of Pd and Sn was measured as [Pd]/[Sn] = 1.25, pointing at a surface segregation of Sn. However, this ratio was much higher in 12 nm Au−Pd2Sn NRs, up to [Pd]/[Sn] = 5.5 when using a 0.02 M AuCl3 concentration to grow the Au tips (Table 1). This experimental result further points toward a galvanic replacement of surface Sn by Au. Fitting each region of the XPS spectra, it could be observed that in Pd2Sn and Au−Pd2Sn NRs, the deconvolution of the Pd 3d spectra indicated the presence of two Pd-oxidation states, a dominant Pd0 state with a doublet at around 335.6 eV (Pd 3d5/2) and 340.9 eV (Pd 3d3/2), and a Pd2+ state with a doublet at 337.6 eV (Pd 3d5/2) and 342.9 eV (Pd 3d3/2). With the Au introduction, these two doublets were slightly shifted to lower BEs (ΔE = −0.5 eV) and an increase of the Pd0 contribution was observed. Larger changes were obtained in the Sn 3d spectral region, which showed three main Sn contributions in Pd2Sn NRs: a main Sn2+ (486.3 and 494.9 eV) and minor Sn4+ (488.4 and 496.8 eV) and Sn0 (484.8 and 493.3 eV) components. Oxidized Sn phases, related either to the Sn

reaction with oxygen or its coordination with ligands, are a common observation on the surface of Pd−Sn and Pt−Sn alloys.45,46 With the introduction of Au, on top of the decrease of the Sn signal described above, the main Sn2+ contribution was further oxidized, shifting its doublet peak position more than 1 eV toward higher BEs. Finally, the deconvolution of the Au 4f spectrum in Au−Pd2Sn showed two doublets. The major contribution corresponded to metallic Au (83.3 and 87.0 eV) and the minor contribution, at higher BEs (84.5 and 88.2 eV), indicated the presence of positively charged gold atoms, Auδ+ , attributed to Au surface atoms with different environments.

The Pd2Sn NR surface chemistry was further elucidated by TGA and solution 1 H NMR after thoroughly washing the NRs. TGA showed the presence of 12% of organics in 10 nm Pd2Sn NRs (Figure S2). In the solution 1 H NMR spectra, the resonance at chemical shift around 5.3 ppm characteristic of the alkene group indicated the presence of OAm (Figures S3 and S4a). The alkene group displayed slightly shifted sharp resonances in the 1 H NMR spectra, in contrast to the broad resonances typically characteristic of tightly bound ligands.42 In parallel, NOESY spectra presented negative cross peaks corroborating the interaction of OAm with the Pd2Sn surface (Figure S4b). These data pointed toward the possibility of a highly dynamic surface stabilization, as previously reported for other systems.47,48 Hence, we studied the diffusion coefficient of our system (NR plus the ligand shell) using DOSY experiments. From DOSY data (Figure S5), a diffusion coefficient of 120 ± 12 μm2 s −1 was obtained for 26 nm Pd2Sn NRs. The diffusion coefficient calculated using the theoretical model of Mansfield and Douglas49 for 26 nm NRs with rounded ends was 26 μm2 s −1 . The much larger diffusion coefficient experimentally measured was ascribed to a highly dynamic binding of OAm on the Pd2Sn NRs surface.

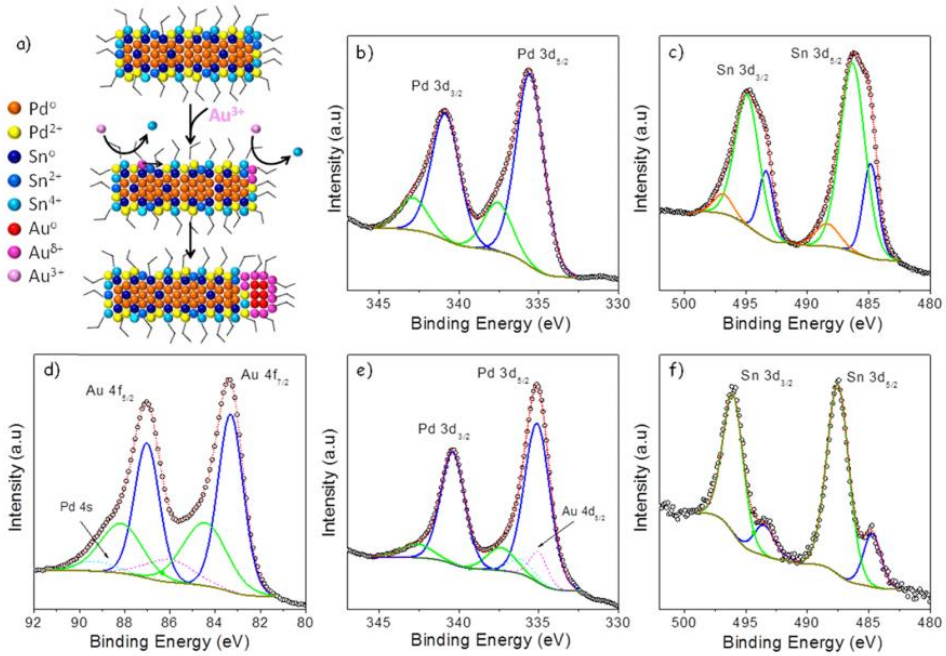

Figure 3. (a) Scheme of the proposed Au−Pd2Sn formation mechanism. (b−f) Detailed regions of the XPS spectra of 10 nm Pd2Sn (b,c) and 12 nm Au−Pd2Sn NRs. (d−f) Pd 3d (b,e), Sn 3d (c,f), and Au 4f (d), as indicated within each graph.

3.2. Hydrogenation Reactions.

The exploration of the catalytic potential of Pd2Sn and Au−Pd2Sn NRs was started with the hydrogenation of styrene to ethylbenzene (Table 2). Pd2Sn NRs were active in the hydrogenation reaction when DCM was used as the solvent, and H2 pressure was set at 3 bar. Pd2Sn NRs (10 nm) achieved conversions above 70% at large substrate loadings (100 g styrene/g Pd2Sn), even under mild reaction conditions (25 °C, Table 2, entry 1). Larger Pd2Sn NRs systematically resulted in lower activities (Table 2, entry 2). We associate this experimental result to their lower surfaceto-bulk ratio and possibly to their reduced density of potentially active sites such as tips. Thus, 10 nm Pd2Sn NRs were used for all following catalytic tests.

Activity was lower at 1 bar of H2 (Table 2, entry 4) and when using methanol as the solvent (Table 2, entry 5) because of the low colloidal stability of the NRs in this solvent. Even at much harsher conditions (Table 2, entry 6), the reaction yielded just ethylbenzene, without any trace of phenyl group hydrogenation. Without solvent, in neat styrene (Table 2, entry 7), the highest TOF values up to 286 h−1 were reached. Overall, TOF values compared favorably to related nanosystems making use of other metals.50

Tables 3 and 4 show results obtained from the hydrogenation of 1-octene and alkynes, namely PhA and 1-octyne, under the optimized conditions set with styrene. In the hydrogenation of 1-octene, apart from the hydrogenated product, octane, isomerization of the substrate to the two geometric isomers of 2-octene was observed. This isomerization depends on the sequence of insertion and β-hydride elimination on the NR surface (Scheme S1). Similar results and tendencies were obtained for the hydrogenation of 1- octyne. On the other hand, in the hydrogenation of PhA, very little amounts of ethylbenzene were formed, evidencing the higher reactivity of PhA compared to styrene in hydrogenation. In terms of the Au effect on hydrogenation reactions, Pd2Sn NRs were considerably more active in the hydrogenation of styrene than Au−Pd2Sn NRs, whereas the opposite trend was observed for 1-octene. The nonconjugated nature of the double bond and the lesser steric shielding of 1-octene compared to styrene could explain this result. In contrast, the differences in performance were less important for PhA and 1- octyne, with Au−Pd2Sn being more active for both substrates. These trends could be understood by the known alkynophilicity of Au.39−41,51 The high electron-rich character of the triple bond probably hid the effect of the substituent. It should be mentioned that all of the comparisons carried out between Pd2Sn and Au−Pd2Sn NRs were based on results obtained from the exact same batch of Pd2Sn NRs.

3.3. Sonogashira Coupling Reaction

Pd2Sn and Au− Pd2Sn NR performance in the Sonogashira reaction between PhA and iodobenzene (phenyl iodide, PhI) to give diphenylacetylene (tolan) is displayed in Table 5. Using Pd2Sn NRs and K2CO3 as the base (Table 5, entries 1−4), very high conversions could be attained at 2 h (Table 5, entry 2). The reaction yielded mainly tolan, although products 1 and 1′ were also formed. Both products were analyzed by GC−MS, providing a peak at m/z of 280 units, what proved that they were isomeric. These compounds arose from the condensation of two molecules of PhA and one molecule of PhI, which gave a pair of geometric isomers of a 1,3-enyne (Figure 4). The decrease of the catalyst loading (Table 5, entry 3) produced a drop on the conversion and selectivity to tolan. The calculated TOF values were similar to those obtained previously from related Pd-nanosytems.9

When the base was changed to KOH (Table 5, entries 5−8), activities significantly increased, achieving full conversion at 1 h (Table 5, entries 5 and 7). However, the selectivity toward tolan

was not improved because apart from 1 and 1′, transstilbene (tSt) was also produced. This compound is the product of the formal addition of H2 to tolan. Interestingly, not even trace amounts of cis-stilbene (cSt) were detected. Additionally, in all of the assays with KOH, a trace quantity of triphenylethene (TPE) was formed, which arose from the combination of a molecule of PhA and two molecules of PhI.

The recyclability of the Pd2Sn NRs in the Sonogashira reactions was studied by precipitating the NPs by centrifugation and using them in successive runs. To the recovered NRs, a new batch of fresh reagents was added to carry out a second catalytic run under the same conditions. A 10% drop in the conversion was observed in the first run, but no change in the selectivity (Figure S6). We associate this drop to non-full recovery of the material in each precipitation step. A partial NR aggregation during the recovery was also observed (Figure S7), which likely reduced the NR catalytic activity (see Supporting Information for details).

An interesting aspect of the catalytic runs was the unexpected formation of the products tSt, 1, 1′, and TPE. To shed light into the formation of these products, we carried out a set of experiments at different conditions (Table 6). It was found that reducing the concentration of PhI fivefold with respect to 0.1 M used in previous experiments improved the selectivity to tolan (Table 6, cf. entries 1 with 2 and 4 with 5) by diminishing the quantity of 1 and 1′ or eliminating it completely in the case of Au−Pd2Sn NRs (Table 6, entry 4). Unexpectedly, with Pd2Sn NRs, increasing the PhI concentration to 0.5 M (Table 6, entry 3) resulted in no trace of tolan but the formation of new products cSt, 1,2-diphenylethane (DPE), TPE, and 2 (Figure S8). A similar result was obtained with Au−Pd2Sn NRs (Table 6, entry 6), but in this case, only traces of DPE were formed, what improved the selectivity toward cSt.

DPE and 2 can be obtained from the formal addition of hydrogen to St and to 1/1′, respectively, whereas St comes from the formal addition of hydrogen to tolan. To understand the origin of the reduced products and the different selectivities of Pd2Sn and Au−Pd2Sn NRs, a sample of tolan was subjected to the catalytic conditions of the Sonogashira coupling (Table 7). Under Sonogashira conditions, Pd2Sn and Au−Pd2Sn NRs catalyzed the reduction of tolan to St, but not to DPE. The reduction was quite selective to the formation of cSt, as it happened when the Sonogashira coupling was carried out at high concentration (Table 6). As no trace of 1/1′ or 2 was detected, it was concluded that the formation of these molecules needed PhI and PhA. Au−Pd2Sn NRs were less active for the reduction of tolan, possibly due to the stronger adsorption of the triple bond to Au.[39−41,51]

From the above data, a mechanism for the formation of the different products could be envisaged (Scheme 1). The formation of the expected tolan through Sonogashira coupling (left in Scheme 1) involved oxidative addition of PhI, transmetallation with PhA, and reductive elimination. The reduction of tolan catalyzed by the Pd2Sn or Au−Pd2Sn NRs lead to the formation of mainly cSt as shown by the data of Table 6 at high concentration and also by experiments of Table 7. An alternative mechanism (right in Scheme 1) might start with an initial insertion of PhA into the Ph−NR bond forming an intermediate. From this intermediate, 1, 1′, St, and TPE could be produced by functionalization of the NRs and reductive elimination (see Scheme S2). It is interesting to note that by this mechanism, tSt, the most thermodynamically stable compound, is mainly formed as shown in Tables 5 and 6.

Although the reduction of both St isomers produces DPE, the selectivity to cSt observed when performing the reactions at high concentration (Table 6) suggested that most of the DPE was formed by the reduction of cSt, shown in the left-hand side of Scheme 1.

Under the Sonogashira catalytic conditions, the formal addition of a molecule of hydrogen to tolan, St, 1, and 1′ was observed. This pointed out that molecular hydrogen, formed by decomposition of DMF,52,53 was probably involved in the reductions. To explore the origin of the added hydrogen atoms, an experiment with DMF-d7 was performed (see Supporting Information). The detection of a mixture of hydrogenated and deuterated reduction products indicated that the solvent provided the required H or D atoms.52,53

Table 2. Results of the Styrene Hydrogenation with Pd_2Sn NRs

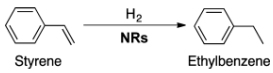

entry	catalyst (size/nm)	solvent	T/°C	P/bar	t/h	loading[a]	conv/%	TOF/h^{-1}
1	Pd_2Sn (10 × 4)	DCM	25	3	1	100	73.3	114
2	Pd_2Sn (40 × 12)	DCM	25	3	1	99	53.3	84
3	Au−Pd_2Sn (12 × 4)	DCM	25	3	1	100	48.3	86
4	Pd_2Sn (10 × 4)	DCM	25	1	1	104	12.8	21
5[b]	Pd_2Sn (10 × 4)	MeOH	25	3	1	103	58.0	96
6	Pd_2Sn (10 × 4)	toluene	70	50	4	30	100	
7[c]	Pd_2Sn (10 × 4)		25	3	1	436	41.3	287

[a]g styrene/g NRs. [b]NRs were poorly soluble in methanol. [c]The reaction was carried out in neat styrene.

Table 3. Results of 1-Octene Hydrogenation with Pd_2Sn and Au−Pd_2Sn NRs[a]

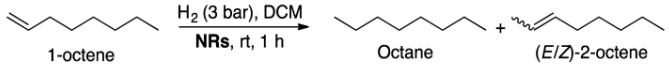

			selectivity/%		
catalyst	conv/%	TOF/h^{-1}	octane	(*E*)-2-octene	(*Z*)-2-octene
Pd_2Sn	70.6	110.2	52.7	27.6	19.7
Au−Pd_2Sn	98.1	157.2	56.7	32.7	10.6

[a]The catalyst loading (g 1-octene/g NRs) was 106.

Table 4. Results of Alkyne Hydrogenation with Pd_2Sn and Au−Pd_2Sn NRs[a]

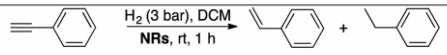

Catalyst	*Conv/%*	*TOF/h^{-1}*	*Selectivity/%*	
			Styrene	*Ethylbenzene*
Pd_2Sn	46.4	78.9	96.6	3.4
Au-Pd_2Sn	54.8	90.7	96.7	3.3

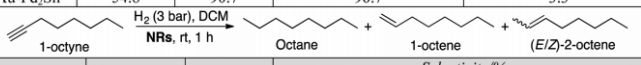

NR	*Conv/%*	*TOF/h^{-1}*	*Selectivity/%*			
			Octane	*1-octene*	*(E)-2-octene*	*(Z)-2-octene*
Pd_2Sn	47.4	75.5	0.0	98.1	1.9	0.0
Au-Pd_2Sn	58.7	93.9	0.7	94.4	4.0	0.9

[a]The catalyst loading (g alkyne/g NRs) was 106.

Table 5. Results of Sonogashira with Pd_2Sn and Au−Pd_2Sn NRs

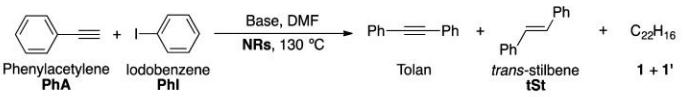

entry	catalyst	base	*t*/h	conv/%	tolan/%	*t*St/%	1 + 1′/%
1	Pd_2Sn	K_2CO_3	1.0	47.2	70.6		29.4
2	Pd_2Sn	K_2CO_3	2.0	97.3	65.7		34.7
3[a]	Pd_2Sn	K_2CO_3	1.0	10.9	40.6		59.4
4	Au−Pd_2Sn	K_2CO_3	1.0	20.9	60.9		39.1
5	Pd_2Sn	KOH	1.0	100	60.8	17.6	21.6
6	Pd_2Sn	KOH	0.5	88.3	66.7	17.9	15.4
7	Au−Pd_2Sn	KOH	1.0	100	65.0	17.0	18.0
8	Au−Pd_2Sn	KOH	0.5	100	67.0	14.1	18.9

[a]5.3 mg of NR were used.

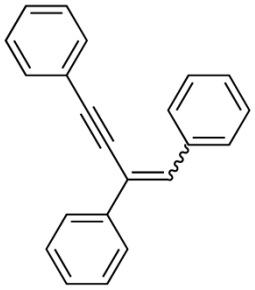

1 + 1'

Figure 4. Proposed structures of 1 and 1′.

Table 6. Effect of the Concentration on the Sonogashira Reaction with NRs

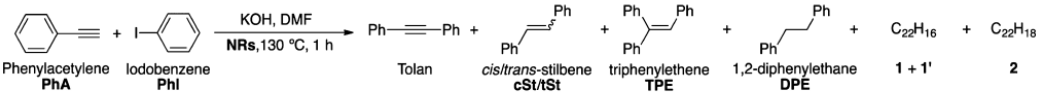

entry	NRs	[PhI]/M	tolan/%	*t*St/%	*c*St/%	TPE/%	DPE/%	1 + 1′/%	2/%
1	Pd_2Sn	0.02	66.7	16.9				16.4	
2	Pd_2Sn	0.1	60.8	17.6				21.6	
3	Pd_2Sn	0.5		10.1	49.2	6.2	9.8	15.2	9.5
4	Au−Pd_2Sn	0.02	88.7	11.3					
5	Au−Pd_2Sn	0.1	65.0	17.0				18.0	
6	Au−Pd_2Sn	0.5		11.9	63.7	3.8		17.5	3.1

Table 7. Results of Tolan Reduction with NRs

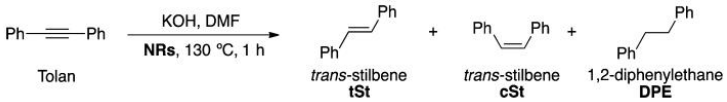

NR[a]	tolan/%	*t*St/%	*c*St/%	DPE/%
Pd_2Sn		10.7	89.3	
Au−Pd_2Sn	33.6	7.1	59.2	

[a]The catalyst loading (g tolan/ g NRs) was 18.

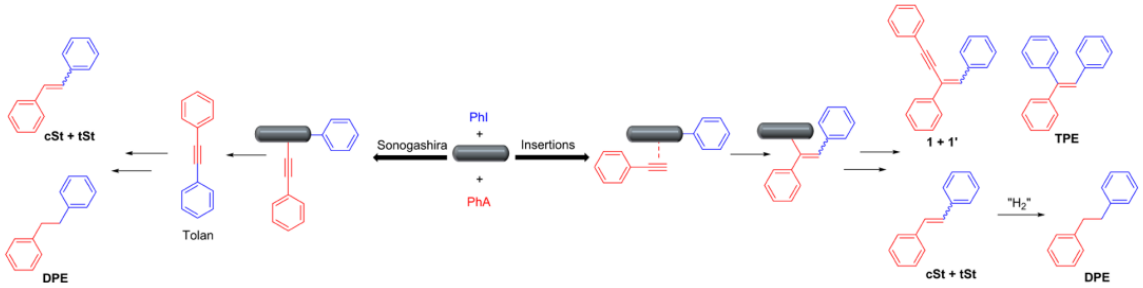

Scheme 1. Mechanisms for the Formation of the Different Products of the Sonogashira Coupling Reaction between PhI and PhA

4. CONCLUSIONS

Au nanodomains were grown at the surface of Pd2Sn NRs through a process involving a galvanic replacement with Sn ions. The surface chemistry of Pd2Sn and Au−Pd2Sn NRs was characterized by XPS and NMR. XPS results evidenced an electron donation from the Pd2Sn NR to the Au tips. Both Pd2Sn and Au−Pd2Sn NRs were found to be very active in the hydrogenation of aromatic and aliphatic alkenes and alkynes under mild conditions. Although Pd2Sn NRs were more active in the hydrogenation of styrene, Au−Pd2Sn NRs performed better for the hydrogenation of alkynes, probably due to their aurophilicity. Pd2Sn and Au−Pd2Sn NRs were also active in the Sonogashira coupling between PhA and PhI to yield tolan in good selectivity, especially with Au−Pd2Sn NRs, when the reaction was performed at high dilution. Interestingly, St was produced at higher concentration either by reduction of tolan or by a mechanism involving insertion of PhA into the NR−Ph bond. In this regard, the production of St can be considered as a cascade or tandem reaction, which was performed with a better selectivity using Au−Pd2Sn NRs as a catalyst. Additionally, the deuterated experiments confirmed that the solvent (DMF) played a role in this cascade reaction. We are currently investigating the implications of this methodology with other substrates.

ACKNOWLEDGMENTS

This work was supported by the European Regional Development Funds and the Spanish MINECO projects ENE2013- 46624-C4-3-R, MAT2014-59961-C2-2-R, and CTQ2015- 65040-P. Z.L. and X.Y. thanks the China Scholarship Council for scholarship support. M.I. thanks AGAUR for Beatriu de Pinos postdoctoral grant (2013 BP-A00344). J.L. is Serra Hunter Fellow and is grateful to ICREA Academia program. Authors also acknowledge the funding from Generalitat de Catalunya 2014 SGR 1638. S.M.-S. acknowledges funding from “Programa Internacional de Becas “la Caixa-Severo Ochoa”. ICN2 acknowledges support from the Severo Ochoa Program (MINECO, Grant SEV-2013-0295). Part of the present work has been performed in the framework of Universitat Autonoma de Barcelona Materials Science PhD program. We would like to thank Michaela Meyns for fruitful discussions.

REFERENCES

(1) Guczi, L. Mechanism of Reactions on Multimetallic Catalysts. J. Mol. Catal. 1984, 25, 13−29.

(2) Mata, J. A.; Hahn, F. E.; Peris, E. Heterometallic Complexes, Tandem Catalysis and Catalytic Cooperativity. Chem. Sci. 2014, 5, 1723−1732.

(3) Buchwalter, P.; Rose, J.; Braunstein, P. Multimetallic Catalysis Based on Heterometallic Complexes and Clusters. Chem. Rev. 2015, 115, 28−126.

(4) Shibasaki, M.; Yamamoto, Y. Multimetallic Catalysts in Organic Synthesis; Wiley-VCH, 2004.

(5) Jia, C.-J.; Schüth, F. Colloidal Metal Nanoparticles as a Component of Designed Catalyst. Phys. Chem. Chem. Phys. 2011, 13, 2457−2487.

(6) Astruc, D.; Lu, F.; Aranzaes, J. R. Nanoparticles as Recyclable Catalysts: The Frontier between Homogeneous and Heterogeneous Catalysis. Angew. Chem., Int. Ed. 2005, 44, 7852−7872.

(7) Balanta, A.; Godard, C.; Claver, C. Pd Nanoparticles for C-C Coupling Reactions. Chem. Soc. Rev. 2011, 40, 4973−4985.

(8) Astruc, D. Palladium Nanoparticles as Efficient Green Homogeneous and Heterogeneous Carbon−Carbon Coupling Precatalysts: A Unifying View. Inorg. Chem. 2007, 46, 1884−1894.

(9) Chu, Y.-T.; Chanda, K.; Lin, P.-H.; Huang, M. H. Aqueous Phase Synthesis of Palladium Tripod Nanostructures for Sonogashira Coupling Reactions. Langmuir 2012, 28, 11258−11264.

(10) Perez-Lorenzo, M. Palladium Nanoparticles as Efficient Catalysts for Suzuki Cross-Coupling Reactions. J. Phys. Chem. Lett. 2012, 3, 167−174.

(11) De Roo, J.; Van Driessche, I.; Martins, J. C.; Hens, Z. Colloidal Metal Oxide Nanocrystal Catalysis by Sustained Chemically Driven Ligand Displacement. Nat. Mater. 2016, 15, 517−521.

(12) Gilroy, K. D.; Ruditskiy, A.; Peng, H.-C.; Qin, D.; Xia, Y. Bimetallic Nanocrystals: Syntheses, Properties, and Applications. Chem. Rev. 2016, 116, 10414−10472.

(13) Flox, C.; Rubio-Garcia, J.; Nafria, R.; Zamani, R.; Skoumal, M.; Andreu, T.; Arbiol, J.; Cabot, A.; Morante, J. R. Active Nano-CuPt3 Electrocatalyst Supported on Graphene for Enhancing Reactions at the Cathode in All-Vanadium Redox Flow Batteries. Carbon 2012, 50, 2372−2374.

(14) Yu, X.; Shavel, A.; An, X.; Luo, Z.; Ibañez, M.; Cabot, A. Cu2ZnSnS4-Pt and Cu2ZnSnS4-Au Heterostructured Nanoparticles for Photocatalytic Water Splitting and Pollutant Degradation. J. Am. Chem. Soc. 2014, 136, 9236−9239.

(15) Nafria, R.; Genc, A.; Iba, ñez, M.; Arbiol, J.; Ramírez de la Piscina, P.; Homs, N.; Cabot, A. Co-Cu Nanoparticles: Synthesis by Galvanic Replacement and Phase Rearrangement during Catalytic Activation. Langmuir 2016, 32, 2267−2276.

(16) Luo, Z. S.; Ibañez, M.; Antolín, A. M.; Genc, A.; Shavel, A.; Contreras, S.; Medina, F.; Arbiol, J.; Cabot, A. Size and Aspect Ratio Control of Pd2Sn Nanorods and Their Water Denitration Properties. Langmuir 2015, 31, 3952−3957.

(17) Xia, X.; Wang, Y.; Ruditskiy, A.; Xia, Y. 25th Anniversary Article: Galvanic Replacement: A Simple and Versatile Route to Hollow Nanostructures with Tunable and Well-Controlled Properties. Adv. Mater. 2013, 25, 6313−6333.

(18) Oh, M. H.; Yu, T.; Yu, S.-H.; Lim, B.; Ko, K.-T.; Willinger, M.- G.; Seo, D.-H.; Kim, B. H.; Cho, M. G.; Park, J.-H.; Kang, K.; Sung, Y.-E.; Pinna, N.; Hyeon, T. Galvanic Replacement Reactions in Metal Oxide Nanocrystals. Science 2013, 340, 964−968.

(19) Anderson, B. D.; Tracy, J. B. Nanoparticle Conversion Chemistry: Kirkendall Effect, Galvanic Exchange, and Anion Exchange. Nanoscale 2014, 6, 12195−12216.

(20) da Silva, A. G. M.; Rodrigues, T. S.; Haigh, S. J.; Camargo, P. H. C. Galvanic Replacement Reaction: Recent Developments for Engineering Metal Nanostructures towards Catalytic Applications. Chem. Commun. 2017, 53, 7135−7148.

(21) Liu, X.; Astruc, D. From Galvanic to Anti-Galvanic Synthesis of Bimetallic Nanoparticles and Applications in Catalysis, Sensing, and Materials Science. Adv. Mater. 2017, 29, 1605305.

(22) Cobley, C. M.; Xia, Y. Engineering the properties of metal nanostructures via galvanic replacement reactions. Mater. Sci. Eng., R 2010, 70, 44−62.

(23) Krylova, G.; Giovanetti, L. J.; Requejo, F. G.; Dimitrijevic, N. M.; Prakapenka, A.; Shevchenko, E. V. Study of Nucleation and Growth Mechanism of the Metallic Nanodumbbells. J. Am. Chem. Soc. 2012, 134, 4384−4392.

(24) Kwon, S. G.; Krylova, G.; Phillips, P. J.; Klie, R. F.; Chattopadhyay, S.; Shibata, T.; Bunel, E. E.; Liu, Y.; Prakapenka, V. B.; Lee, B.; et al. Heterogeneous Nucleation and Shape Transformation of Multicomponent Metallic Nanostructures. Nat. Mater. 2015, 14, 215−223.

(25) The Handbook of Homogeneous Hydrogenation; de Vries, J. G., Elsevier, C. J., Eds.; Wiley-VCH Verlag GmbH, 2008.

(26) Karak, M.; Barbosa, L. C. A.; Hargaden, G. C. Recent Mechanistic Developments and next Generation Catalysts for the Sonogashira Coupling Reaction. RSC Adv. 2014, 4, 53442−53466.

(27) Freakley, S. J.; He, Q.; Harrhy, J. H.; Lu, L.; Crole, D. A.; Morgan, D. J.; Ntainjua, E. N.; Edwards, J. K.; Carley, A. F.; Borisevich, A. Y.; et al. Palladium-tin catalysts for the direct synthesis of H2O2 with high selectivity. Science 2016, 351, 965−968.

(28) Negishi, E.-i.; Anastasia, L. Palladium-Catalyzed Alkynylation. Chem. Rev. 2003, 103, 1979−2018.

(29) Lopez, N.; Vargas-Fuentes, C. Promoters in the Hydrogenatioń of Alkynes in Mixtures: Insights from Density Functional Theory. Chem. Commun. 2012, 48, 1379−1391.

(30) Sales, E. A.; Jove, J.; de Jesus Mendes, M.; Bozon-Verduraz, F. Palladium, Palladium-Tin, and Palladium-Silver Catalysts in the Selective Hydrogenation of Hexadienes: TPR, Mössbauer, and Infrared Studies of Adsorbed CO. J. Catal. 2000, 195, 88−95.

(31) Pattamakomsan, K.; Ehret, E.; Morfin, F.; Gelin, P.; Jugnet, Y.;́ Prakash, S.; Bertolini, J. C.; Panpranot, J.; Aires, F. J. C. S. Selective Hydrogenation of 1,3-Butadiene over Pd and Pd-Sn Catalysts Supported on Different Phases of Alumina. Catal. Today 2011, 164, 28−33.

(32) Hugon, A.; Delannoy, L.; Louis, C. Supported gold catalysts for selective hydrogenation of 1,3-butadiene in the presence of an excess of alkenes. Gold Bull. 2008, 41, 127−138.

(33) Gonzalez-Arellano, C.; Abad, A.; Corma, A.; García, H.;́ Iglesias, M.; Sanchez, F. Catalysis by gold(I) and gold(III): Á Parallelism between Homo- and Heterogeneous Catalysts for CopperFree Sonogashira Cross-Coupling Reactions. Angew. Chem., Int. Ed. 2007, 46, 1536−1538.

(34) Antunes, O.; De Souza, R.; Bittar, M.; Mendes, L.; Da Silva, C.; Da Silva, V. Copper-Free Sonogashira Reaction Using Gold Nanoparticles Supported on Ce2O3, Nb2O5 and SiO2 under Microwave Irradiation. Synlett 2008, 1777−1780.

(35) Beaumont, S. K.; Kyriakou, G.; Lambert, R. M. Identity of the Active Site in Gold Nanoparticle-Catalyzed Sonogashira Coupling of Phenylacetylene and Iodobenzene. J. Am. Chem. Soc. 2010, 132, 12246−12248.

(36) Kanuru, V. K.; Kyriakou, G.; Beaumont, S. K.; Papageorgiou, A. C.; Watson, D. J.; Lambert, R. M. Sonogashira Coupling on an Extended Gold Surface in Vacuo: Reaction of Phenylacetylene with Iodobenzene on Au(111). J. Am. Chem. Soc. 2010, 132, 8081−8086.

(37) Venkatesan, P.; Santhanalakshmi, J. Designed Synthesis of Au/ Ag/Pd Trimetallic Nanoparticle-Based Catalysts for Sonogashira Coupling Reactions. Langmuir 2010, 26, 12225−12229.

(38) Corma, A.; Juarez, R.; Boronat, M.; Sa´ nchez, F.; Iglesias, M.; García, H. Gold Catalyzes the Sonogashira Coupling Reaction without the Requirement of Palladium Impurities. Chem. Commun. 2011, 47, 1446−1448.

(39) Corma, A.; Garcia, H. Supported Gold Nanoparticles as Catalysts for Organic Reactions. Chem. Soc. Rev. 2008, 37, 2096− 2126.

(40) García-Mota, M.; Cabello, N.; Maseras, F.; Echavarren, A. M.; Perez-Ramírez, J.; Lopez, N. Selective Homogeneous and Heteroge- neous Gold Catalysis with Alkynes and Alkenes: Similar Behavior, Different Origin. ChemPhysChem 2008, 9, 1624−1629.

(41) Stratakis, M.; Garcia, H. Catalysis by Supported Gold Nanoparticles: Beyond Aerobic Oxidative Processes. Chem. Rev. 2012, 112, 4469−4506.

(42) Hens, Z.; Martins, J. C. A Solution NMR Toolbox for Characterizing the Surface Chemistry of Colloidal Nanocrystals. Chem. Mater. 2013, 25, 1211−1221.

(43) Sinnaeve, D. The Stejskal-Tanner equation generalized for any gradient shape-an overview of most pulse sequences measuring free diffusion. Concepts Magn. Reson., Part A 2012, 40, 39−65.

(44) Connell, M. A.; Bowyer, P. J.; Adam Bone, P.; Davis, A. L.; Swanson, A. G.; Nilsson, M.; Morris, G. A. Improving the Accuracy of Pulsed Field Gradient NMR Diffusion Experiments: Correction for Gradient Non-Uniformity. J. Magn. Reson. 2009, 198, 121−131.

(45) Du, W.; Mackenzie, K. E.; Milano, D. F.; Deskins, N. A.; Su, D.; Teng, X. Palladium-Tin Alloyed Catalysts for the Ethanol Oxidation Reaction in an Alkaline Medium. ACS Catal. 2012, 2, 287−297.

(46) Lee, A. F.; Baddeley, C. J.; Hardacre, C.; Moggridge, G. D.; Ormerod, R. M.; Lambert, R. M.; Candy, J. P.; Basset, J.-M. Structure−Reactivity Correlations in the Catalytic Coupling of Ethyne over Novel Bimetallic Pd/Sn Catalysts. J. Phys. Chem. B 1997, 101, 2797−2805.

(47) De Roo, J.; Ibañ˜ez, M.; Geiregat, P.; Nedelcu, G.; Walravens, W.; Maes, J.; Martins, J. C.; Van Driessche, I.; Kovalenko, M. V.; Hens, Z. Highly Dynamic Ligand Binding and Light Absorption Coefficient of Cesium Lead Bromide Perovskite Nanocrystals. ACS Nano 2016, 10, 2071−2081.

(48) Liu, Y.; Cadavid, D.; Ibañ˜ez, M.; De Roo, J.; Ortega, S.; Dobrozhan, O.; Kovalenko, M. V.; Cabot, A. Colloidal AgSbSe2 nanocrystals: surface analysis, electronic doping and processing into thermoelectric nanomaterials. J. Mater. Chem. C 2016, 4, 4756−4762.

(49) Mansfield, M. L.; Douglas, J. F. Transport Properties of Rodlike Particles. Macromolecules 2008, 41, 5422−5432.

(50) Wu, Y.; Cai, S.; Wang, D.; He, W.; Li, Y. Syntheses of WaterSoluble Octahedral, Truncated Octahedral, and Cubic Pt-Ni Nanocrystals and Their Structure-Activity Study in Model Hydrogenation Reactions. J. Am. Chem. Soc. 2012, 134, 8975−8981.

(51) Segura, Y.; Lopez, N.; Perezramirez, J. Origin of the Superior Hydrogenation Selectivity of Gold Nanoparticles in Alkyne + Alkene Mixtures: Triple- versus Double-Bond Activation. J. Catal. 2007, 247, 383−386.

(52) Yoo, B.-S.; Choi, N.-S.; Yong Shim, C.; Son, Y.; Lee, S. W. Electrophilic attack of alkyl halide at the cyanide nitrogen in trans- [Fe(H)(CN)(dppe)2]: preparation, structure, and properties of trans-[Fe(H)(CNR)(dppe)2]X (dppe=Ph2PCH2CH2PPh2; R=Me, Et, Pr, i-Pr, n-Bu, CH2CH2Br, CH2CH2CH2I, CH2CHCH2, CH2CCH; X=Br, I). Inorg. Chim. Acta 2000, 309, 137−145.

(53) Wang, H.-S.; Wang, Y.-C.; Pan, Y.-M.; Zhao, S.-L.; Chen, Z.-F. Simultaneous Reduction of Nitro- to Amino-Group in the PalladiumCatalyzed Suzuki Cross-Coupling Reaction. Tetrahedron Lett. 2008, 49, 2634−2637.